Blocking Losses On An Optical Communications Link

Bruce Moision, Sabino Piazzolla
Jet Propulsion Laboratory, California Institute of Technology, 4800 Oak Grove Drive, Pasadena, CA 91109
bruce.moision,sabino.piazzolla@jpl.nasa.gov

***Abstract*—Many photon-counting photo-detectors have the property that they become inoperative for some time after detection event. We say the detector is *blocked* during this time. Blocking produces losses when using the detector as a photon-counter to detect a communications signal. In this paper, we characterize blocking losses for single detectors and for arrays of detectors. For arrays, we discuss conditions under which the output may be approximated as a Poisson point process, and provide a simple approximation to the blocking loss. We show how to extend the analysis to arrays of non-uniformly illuminated arrays.**

I. Introduction

Many photon-counting photo-detectors have the property that they become inoperative for some time after detection event. We say the detector is *blocked* during this time. When used to detect a communications signal, blocking leads to losses relative to an ideal detector, which may be measured as a reduction in the communications rate for a given received signal power, or a required increase in the signal power required to effect the same communications rate In this paper, we characterize blocking losses for single detectors and for arrays of detectors.

Throughout we assume the communications signal is intensity modulated, and received by an array of photon-counting photo-detectors. For the purpose of this analysis, we assume the detectors are ideal, in that they produce a signal that allows one to reproduce the arrival times of electrons, produced either as photo-electrons or from dark noise, exactly. For single detectors, we illustrate the performance of the maximum-likelihood(ML) receiver in blocking, as well as a *maximum-count*(MC) receiver, that, when receiving a pulse-position-modulated(PPM) signal, selects the symbol corresponding to the slot with the largest electron count. We show that whereas the MC receiver saturates at high count rates, the ML receiver may not. We numerically compute the loss in capacity, symbol-error-rate, and count-rate. We show that the capacity and symbol-error-rate losses track, whereas the count-rate loss does not, generally, reflect the SER or capacity loss, as the slot-statistics at the detector output are no longer Poisson. We show that the MC receiver loss may be accurately predicted for dead-times on the order of a slot, by using the exact statistics provided in [1].

Blocking may be mitigated by spreading the signal intensity over an array of detectors, reducing the count rate on any one detector. We discuss conditions under which the sum of the arrayed detectors may be approximated as a Poisson point process, and provide a simple approximation to the blocking loss as a function of the probability that a detector is unblocked at a given time, essentially treating the blocking probability as a scaling of the detection efficiency. We show how to extend the analysis to arrays of non-uniformly illuminated arrays.

We also discuss incorporating a more accurate model of the blocking phenomenon, wherein the detector is blocked for some time, then has a recovery of its detection efficiency to the steady-state value. We illustrate in the Appendix how to accurately model the reduction in count rate for such a detector, and show that the additional loss due to the recovery may be modeled by extending the blocking duration.

II. Channel Model

Suppose we are transmitting data over an optical link via intensity modulation with pulse-position-modulation (PPM) of order M and slot width T_s. The signal, received on an array of K detectors, is modeled as a Poisson point process. The incident photon flux on the jth detector is

$$l_j(t) = l_b/K + l_s q_j M \sum_i u(t - T_s(x_i + iM))$$

where l_b and l_s are the cumulative background and signal rates over the entire array, q_j is fraction of the signal incident on the jth detector ($q_j \in [0,1]$, $\sum_j q_j = 1$), $u(t)$ is a unit pulse on $[0, T_s)$ ($u(t) = 1/T_s$ on $[0, T_s]$, and $u(t) = 0$ elsewhere), and $x_i \in \{0, 1, \ldots, M-1\}$ is the pulse position of the ith symbol. We assume the distribution $\mathbf{q} = (q_1, \ldots, q_K)$ is constant. In general, the signal intensity pattern would be time-varying due to random changes in the optical phase front. However, in our cases of interest the coherence time of these variations is much longer than the symbol durations.

Let η be the detection efficiency, and l_d the detector dark rate. We assume a perfect detector/receiver, that reproduces the arrival time of each detected photo-electron or dark-current electron. In the remainder, we refer to all events at the output of the detector as electrons. Each detector is paralyzed, or blocked, following the detection of an electron for a duration τ seconds[1] during which no electrons are produced. Due to

[1] A more accurate model for some detectors is that the detection efficiency recovers exponentially. This will be treated in Section V-B1 and Appendix A.

the blocking, the output process is a self-excited point process. Let $N_j(t)$ denote the number of electrons produced by the jth detector on $[0,t)$, $\{w_1, w_2, \ldots, w_{N_j(T)}\}$ their ordered arrival times ($w_i < w_{i+1}$), and

$$\nu_j(t) = \eta l_j(t) + l_d$$

the intensity function of the unblocked electron process (the intensity of electrons in the absence of blocking). Suppose we observe arrivals over an interval $[0,T]$. The detector output sample function density, conditioned on l_j is [2]

$$p(\{N_j(t), 0 \le t \le T\}|l_j) =$$
$$\begin{cases} \exp\left(-\int_0^T \nu_j(t)dt\right) & , N_j(T) = 0 \\ \prod_{i=1}^{N_j(T)} \nu_j(w_i) \exp\left(-\sum_{i=1}^{N_j(T)+1} \int_{w_{i-1}+\tau}^{w_i} \nu_j(t)dt\right) & , \text{otherwise} \end{cases}$$

where, for notational convenience, we define $w_0 \stackrel{\text{def}}{=} -\tau$ and $w_{n+1} \stackrel{\text{def}}{=} T$.

The point processes produced by each detector are conditionally independent. Letting $\mathbf{N}(t) = (N_1(t), \ldots, N_K(t))$ and $\mathbf{l} = (l_1, \ldots, l_K)$, the joint statistics of the detected process are

$$P(\{\mathbf{N}(t), 0 \le t \le T\}|\mathbf{l}) = \prod_{j=1}^{K} p(\{N_j(t), 0 \le t \le T\}|l_j)$$

III. Single Detector

We first consider reception of the signal with a single detector ($K = 1, q_1 = 1.0$). In the single detector case, we make the simplifying assumption in analysis that the detector is unblocked at the beginning of each PPM symbol. This effectively removes inter-symbol-interference (ISI), and restricts applicability to cases where the blocking duration is less than a channel symbol. It will allow us to find simple expressions for the maximum-likelihood(ML) symbol-error-rate (SER) and the channel capacity, which would otherwise be complicated by the presence of ISI. We also set $l_d = 0$.

A. Symbol Error Rates

The ML symbol decision is given by

$$\hat{x}_{\text{ML}} = \arg \max_{x \in \{0,1,\ldots,M-1\}} p(N(t)|x)$$

where, to emphasize the symbol decision, we condition on the symbol position x, which completely specifies $l(t)$. Let n_j denote the number of counts in the jth slot (the interval $[(j-1)T_s, jT_s)$). In the absence of blocking, the collection of slot counts are a sufficient statistic for ML detection, and the ML decision reduces to selecting the slot with the maximum count. It's instructive to observe the behavior of this max-count(MC) receiver in the presence of blocking. Let

$$\hat{x}_{\text{MC}} = \arg \max_{x \in \{0,1,\ldots,M-1\}} n_x$$

Figure 1 illustrates the symbol error rate, $P_s = P[\hat{x} \neq x]$, of the ML receiver, the MC receiver, and an unblocked receiver ($\tau = 0$), for the case $M = 16$, $\tau = 1.0$ ns, $l_b = 1.0e8$ photons/sec, $l_d = 0$, and $T_s = 2$ ns.

We also plot two analytic approximations to the MC receiver. The first approximation uses the true probability mass functions of noise and signal slots provided in [1]. However, it assumes the slot counts are independent. For τ small relative to MT_s, the independence assumption is reasonable, and the approximation is accurate. The second approximation assumes the slot counts are Poisson distributed, using the measured signal and noise slot mean count rates. We see that the Poisson assumption is inaccurate.

B. Capacity

The capacity of the channel (assuming the receiver has access to all detection event times) with a input drawn uniformly on $\{1, \ldots, M\}$ is given by [3]

$$C_{\text{PPM}} = \frac{1}{MT_s} E_{X,N_t}\left[\log_2 \frac{\exp(L(N(t)|X))}{\frac{1}{M}\sum_j \exp(L(N(t)|x=j))}\right] \text{ bits/s}$$

where $E_{X,N(t)}$ is an expectation over X and $N(t)$, and $L(N(t)|x) = \log p(N(t)|x)$. Figure 2 illustrates the capacity, evaluated numerically, as a function of l_s for $M = 16$, $\tau = 1.0$ ns, $l_b = 10^8$ photons/sec, $l_d = 0$, and $T_s \in \{0.5, 1.0, 2.0, 4.0\}$ ns. At large signal power, the capacity approaches the same limit as for the unblocked case, $\log_2(M)/(MT_s)$. We can see this intuitively, since there is information conveyed in the inter-arrival-times, not only the slot counts, and the inter-arrival-times in a signal slot can be reduced by increasing the signal power.

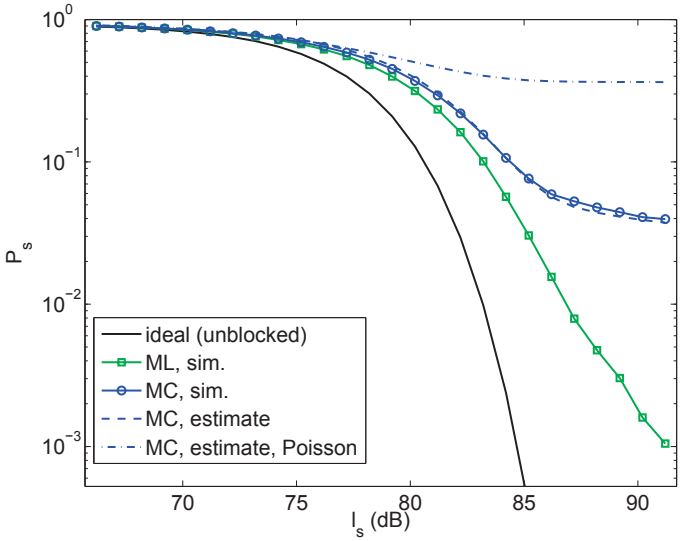

Fig. 1. Symbol Error Rates for a single blocked detector, with ML (unblocked and blocked) and MC symbol decisions. Also illustrated are two approximations to the MC error rate. $M = 16$, $T_s = 2.0$ ns, $\tau = 1.0$ ns, $\lambda_b = 10^8$ photons/s

C. Assessing Losses

Figure 3 illustrates several measures of the blocking loss for the case $T_s = 2$ ns, $\tau = 1$ ns, $l_d = 0$ and $l_b = 10^8$ photons/s.

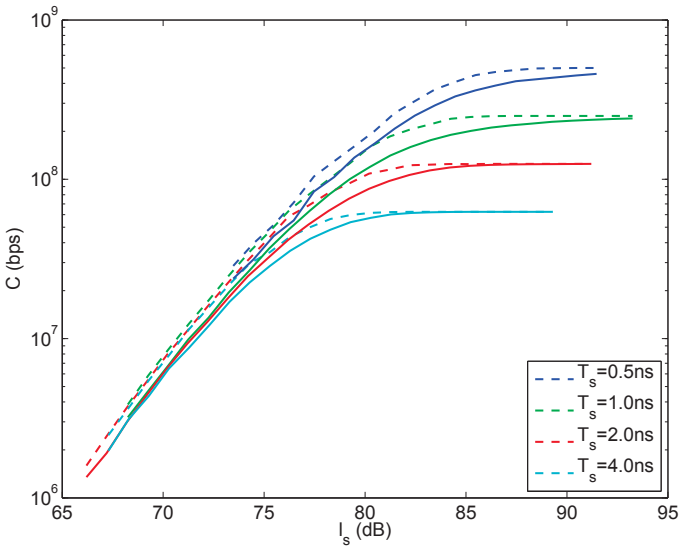

Fig. 2. Capacity, solid lines are blocked capacities, dashed unblocked. Varying T_s with $M = 16$, $\tau = 1.0$ ns, $\lambda_b = 10^8$ photons/s for all.

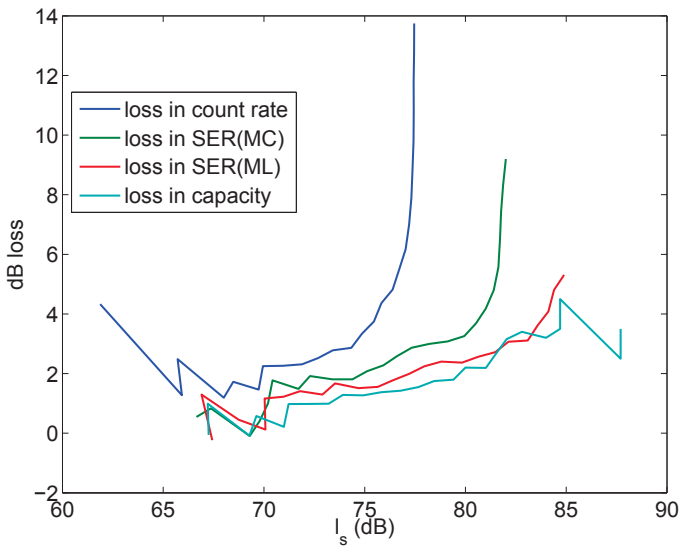

Fig. 3. Blocking Losses measured in terms of count rate, MC SER, ML SER and Capacity (ML). $M = 16$, $T_s = 2.0$ ns, $l_d = 0$, $l_b = 10^8$ photons/s, $\tau = 1.0$ ns

The loss in SER and capacity are the dB increase in l_s required to affect the same SER or capacity as an unblocked detector. The loss in count rate is the difference between the incident signal rate, l_s, and the signal count rate at the detector output.

We see that the ML SER loss tracks well with the capacity loss. We expect that the capacity of the MC receiver would also track with the MC SER loss. The plots show that the ML receiver achieves a gain over the MC receiver (a lower signal power to achieve the same SER), although the gains diminish at low SER. The SER and count-rate losses grow unbounded at high signal power, whereas, as noted earlier, the capacity loss goes to zero at high power (a discontinuity in the limit).

How should the loss be assessed? The relevant loss is the increase in signal power required to transmit data at a specified error rate. We assume the information bits are encoded with a power efficient error-correction-code prior to being mapped to PPM symbols. Suppose the systems use codes of rate $1/2$. The relevant operating point then corresponds to a capacity $\log_2(M)/(2MT_s)$. Modern ECCs can achieve acceptably low error rates at signal powers $\approx$ 2 dB in excess of capacity (accounting for implementation losses). In cases where the capacity is difficult to measure, we take the loss corresponding to a target uncoded SER of $0.2(M-1)/(M/2)$, corresponding to information bit-error-rate (post-decoding) of $\approx 10^{-6}$. Utilizing the SER as a measure has the advantage that the SER may be estimated directly via simulation when analytical expressions are intractable.

For example, in Figure 3, the relevant range of λ_s, from Figure 2, would be ≈ 78 dB. Here the error in using an MC receiver, for example, is less pronounced.

IV. Multiple Detectors

In most practical cases, the signal will be focused on an array of detectors. This enables pointing and tracking algorithms and spatial filtering. For detectors with blocking, spreading the signal over many detectors lowers the signal intensity per detector, mitigating blocking (presuming blocking is dominated by the signal). In this section we extend the single detector analysis to multiple detectors.

Although the ML receiver is of theoretical interest, in practice it may be prohibitively complex to implement. Figures 4 and 5 illustrate the MC SER relative to the unblocked SER. In these simulations, we no longer assume the detector is initially unblocked. Also illustrated are several approximations to the SER. These are described in the following section.

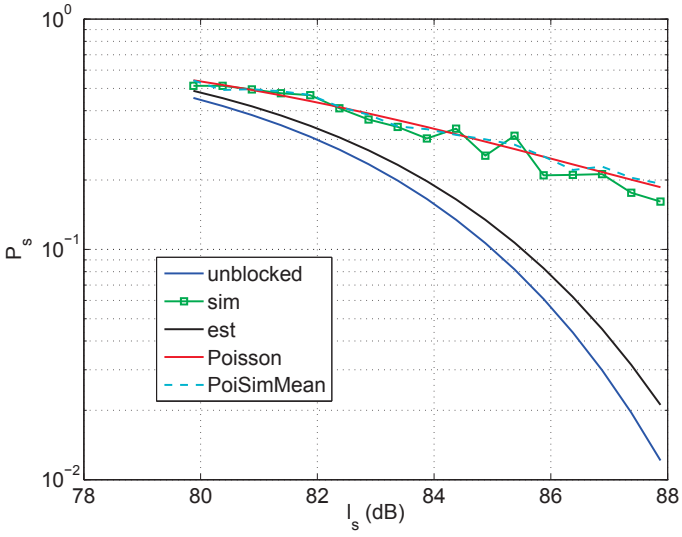

Fig. 4. Blocking Losses $M = 8$, $T_s = 1.0$ ns, $l_b = 10^7$ p/s, $l_d = 10^3$ pe/s, $\eta = 0.3$, $K = 16$, $\tau = 48.0$ ns

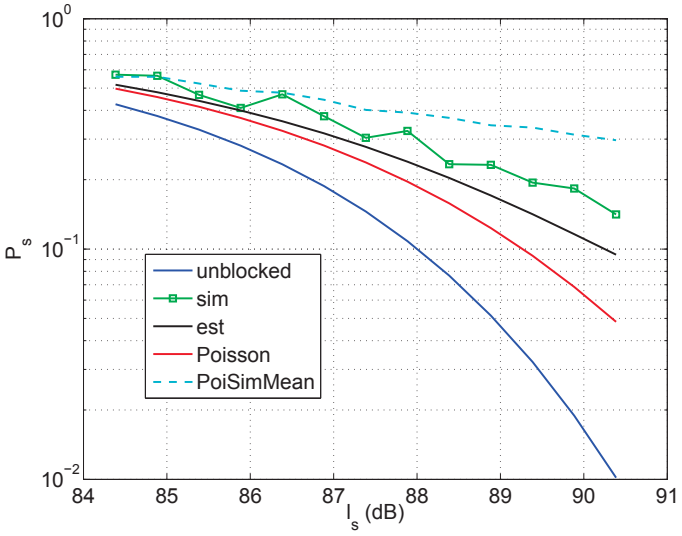

Fig. 5. Blocking Losses $M = 8$, $T_s = 1.0$ ns, $l_b = 10^9$ p/s, $l_d = 10^3$ pe/s, $K = 4$, $\tau = 1.0$ ns

V. Predicting Blocking Loss

In this section we derive some methods to predict the blocking loss.

A. Non-Poisson Statistics

Slot statistics in the presence of blocking are derived in [1]. This analysis may be extended to arrays of detectors as follows. Let $N_j^{(i)}$ be the number of counts in the ith slot of the jth detector, $p_{0,j}(k) = P(N_j^{(i)}|x \neq i)$ and $p_{1,j}(k) = P(N_j^{(i)}|x = i)$ the probability mass functions of a noise and signal slot, respectively, where x is the pulse position. These mass functions, under the approximation that every slot is preceded by an un-pulsed slot, were derived in [1]. Let $N_i = \sum_{j=1}^{K} N_j^{(i)}$, the summed count. Since the arrival processes are independent, we have

$$p_0(k) := P(N_i = k|x \neq i) = \underset{j=1}{\overset{K}{*}} p_{0,j}(k) \tag{1}$$

$$p_1(k) := P(N_i = k|x = i) = \underset{j=1}{\overset{K}{*}} p_{1,j}(k) \tag{2}$$

where $*$ denotes convolution.

Using the exact slot statistics, and assuming independent slot counts, provides accurate estimates of the MC receiver performance when the blocking duration is on the order of the slot duration, as illustrated in Figure 1 for a single detector, and Figure 5. However, the mass functions in [1] do not account for inter-symbol-interference, and the independence assumption breaks down for long durations. In the following sections, we develop a Poisson approximation, which will prove to be accurate in many cases of interest.

B. Blocking Probability

Suppose the unblocked electron rate of the detector is a constant l, and divide time into intervals of δ seconds. We may approximate the evolution of the detector state with an $L = \tau/\delta$ state Markov chain, illustrated in Figure 6. State 0 is the unblocked state. With probability $q_0 = \exp(-\delta l)$, no photons are detected and the detector remains unblocked. If photons are detected, the detector remains blocked for $L\delta = \tau$ seconds. Let μ_0 denote the probability the detector is in the unblocked state. We have

$$\begin{aligned}\mu_0 &= \frac{1}{1 + Lq_1} \\ &= \frac{1}{1 + \frac{\tau}{\delta}(1 - e^{-\delta l})}\end{aligned}$$

and, in the limit of small δ,

$$\mu_0 = \frac{1}{1 + \tau l} \tag{3}$$

Adding memory to the modulation, via PPM, will increase the blocking probability [4]. Nonetheless, we may model the probability that the detector is blocked at some time t as a stationary μ_0.

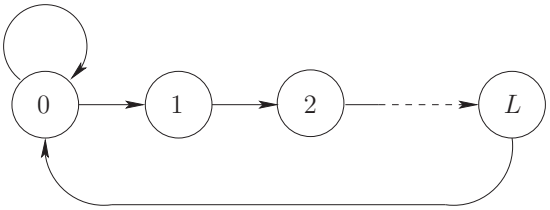

Fig. 6. Markov model of detector state

1) Adjustment for Exponential Recovery: A more accurate model of blocking for certain detectors is as a time-varying detection efficiency that goes to zero for a period of τ seconds after the production of a photo-electron, and then rises exponentially, with time constant τ_b, back to its maximum value of η_0. That is, if the last detected event was at time s, the detection efficiency at time t is

$$\eta(t) = \eta_0 \left(1 - \exp(-\max(0, t - s - \tau)/\tau_b)\right) \tag{4}$$

An example with $\eta_0 = 0.5$, $\tau_b = 0.5T_s$ and $\tau = 0.2T_s$ is illustrated in Figure 7

We may model the exponential recovery by extending the blocking duration such that the mean detected photo-electrons over the duration of the recovery is preserved. That is, we take the blocking duration to be $\tau' = \tau + \tau_b$, so that, with $s = 0$,

$$\lim_{T\to\infty} \left(\eta_0(T - \tau') - \int_0^T \eta(t)dt \right) = 0$$

C. Poisson Approximation: Sums of Point Processes

The sum of a collection of independent, uniformly sparse point processes converges in distribution to a Poisson point process [2, Theorem 5.2.3]. This suggests approximating the summed process as Poisson. But how quickly does this converge, and how does it converge if the component processes are not sparse?

We consider the accuracy of the Poisson approximation by examining the statistics of a count over a finite interval. Let

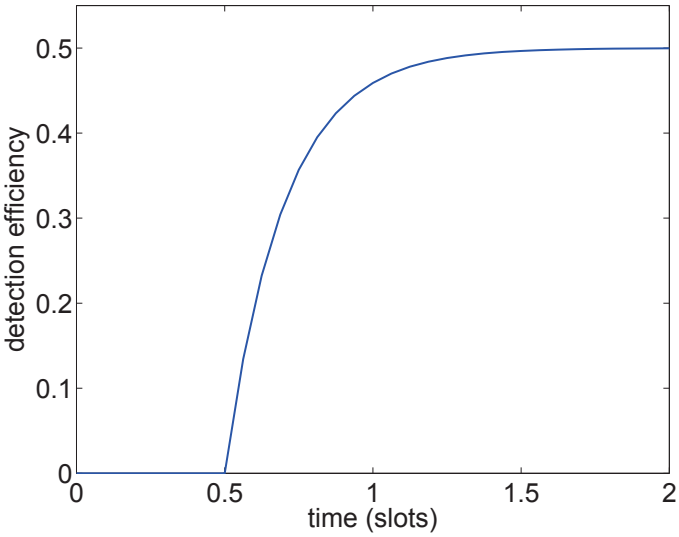

Fig. 7. Detection Efficiency–Recovery from a Detection Event at $s = 0$

Y_i be the count over an interval $\epsilon \leq \tau$ from detector i, and let $S_K = \sum_{i=1}^{K} Y_i$ be the sum of the counts over the interval. The sum S_K converges in distribution to a Poisson random variable with mean $\sum_{i=1}^{K} p_i$ where $p_i = P[Y_i = 1]$ [5]. Suppose the unblocked electron process on the ith detector has a constant intensity l_i. One can show that

$$p_i = \frac{\delta l_i}{1 + \tau l_i}$$

The divergence between the distribution of S_K, P_{S_K}, and a Poisson random variable with mean λ, $Po(\lambda)$, may be bounded as [5]

$$D(P_{S_K}||Po(\lambda)) \leq \frac{1}{\sum_{i=1}^{K} p_i} \sum_{i=1}^{K} \frac{p_i^3}{1 - p_i}$$

Suppose $l_1 = l_2 = \cdots = l_K$. Put $\delta = \tau$, the maximum duration over which the Y_i are binary. Then we have

$$D(P_{S_K}||Po(\lambda)) \leq \frac{(\tau l_1)^2}{(1 + \tau l_1)}$$

As we would expect, the Poisson approximation becomes more accurate with decreasing mean counts per detector per dead-time (quadratically in τl_1 for small τl_1) and less accurate with increasing τl_1 (linear in τl_1 for large τl_1). In particular, we are interested in how well a slot count is approximated as Poisson-distributed. Suppose $T_s \ll \tau$, put $\delta = T_s$, and use the approximation $(1 + l_1(\tau - T_s)) \approx (1 + l_1\tau)$. Then

$$D(P_{S_K}||Po(\lambda)) \leq \left(\frac{T_s l_1}{1 + \tau l_1} \right)^2$$

Hence we may expect the Poisson approximation over a slot to be accurate even for large τl_1, so long as the mean counts per detector per slot time is small.

D. Poisson Approximation: Channel Capacity

In this section, following the treatment in [6], we derive an approximate loss given the Poisson approximation in Section V-C holds. Consider the channel in the absence of blocking, with mean signal photo-electron rate ηl_s and mean noise rate $\eta l_b + K l_d$. One may bound the PPM capacity by the capacity of an intensity modulated channel with the same duty cycle, $1/M$, and infinite bandwidth. This bound is a good approximation to the PPM capacity, and losses computed based on it will prove to accurately reflect PPM losses. The capacity of the unblocked intensity modulated Poisson channel with duty cycle $1/M$ is given by [7]

$$C_u = \eta l_s f(\rho) \text{ bits/s}$$

where

$$f(\rho) = \left(1 + \frac{1}{M\rho}\right) \log_2(1 + M\rho) - \left(1 + \frac{1}{\rho}\right) \log_2(1 + \rho)$$
$$\rho = \frac{\eta l_s}{\eta l_b + K l_d}$$

We will find it useful to use the approximation [8]

$$C_u \approx \eta l_s g(\rho)$$

where

$$g(\rho) \stackrel{\text{def}}{=} \frac{\log_2 M}{1 + \frac{1}{\rho} \frac{2 \log M}{M - 1}}$$

In the presence of blocking, we may treat the probability that the detector is unblocked as a scaling of the detection efficiency, and approximate the signal and noise rates as

$$l_s' = \eta l_s \sum_{i=1}^{K} \frac{q_i}{1 + \tau l_i} \tag{5}$$

$$l_b' = (\eta l_b / K + l_d) \sum_{i=1}^{K} \frac{1}{1 + \tau l_i} \tag{6}$$

and approximate the capacity as

$$C_b \approx l_s' g(\rho')$$

where

$$\rho' = \rho \frac{\sum_{i=1}^{K} \frac{q_i}{1 + \tau l_i}}{\sum_{i=1}^{K} \frac{1}{K} \frac{1}{1 + \tau l_i}}$$

Suppose the illumination is uniform: $q_1 = q_2 = \cdots = q_K$, and, subsequently, $l_1 = l_2 = \cdots l_K$. Then $\rho' = \rho$ and the capacity loss is

$$\frac{C_b}{C_u} \approx \frac{1}{1 + \tau l_1}$$

So we lose, due to blocking, approximately μ_0 bits/s, the fraction of time a detector is unblocked. We may also state the loss in terms of the increase in signal power required to achieve the same capacity. Putting

$$C_u \approx \eta l_s g(\rho) = \eta l_s' \mu_0 g(\rho) \approx C_b$$

and solving for l_s in terms of l'_s yields

$$l_s = \frac{\mu_0 l'_s + \sqrt{(\mu_0 l'_s)^2 + 4\mu_0\psi(l'_s+\psi)}}{2(1+\psi/l'_s)}$$

where

$$\psi = \frac{2\log M(\eta l_b + K l_d)}{\eta(M-1)}$$

Hence the loss is

$$\text{loss} \stackrel{\text{def}}{=} \frac{l'_s}{l_s} = \frac{2(\psi+l'_s)}{\mu_0 l'_s + \sqrt{(\mu_0 l'_s)^2 + 4\mu_0\psi(l'_s+\psi)}} \quad (7)$$

We may simplify the loss in the region where either the signal is dominant (high 'SNR') or the noise is dominant (low 'SNR'). Suppose $\psi \gg l'_s$ (low SNR), then we have

$$\text{loss} \approx \frac{1}{\sqrt{\mu_0}}$$

Alternately, if $\psi \ll l'_s$ (high SNR), we have

$$\text{loss} \approx \frac{1}{\mu_0}$$

We can also see this by noting that the capacity goes as $(l'_s)^2/(l'_s+l'_b)$. To the extent that blocking is well modeled as a scaling of the detection efficiency by μ_0, at high SNR this yields a loss of μ_0, and at low SNR a loss of $\sqrt{\mu_0}$.

E. Poisson Approximation: Accuracy

Returning to the more general model in Section V-B1, Figure 8 illustrates an example with $K = 16$, $l_b = 1.6 \times 10^9$ p/s, $l_d = 10^3$ e/s, $T_s = 1$ ns, $M = 8$, $\tau = 8T_s$, $\tau_b = 16T_s$, and $\eta = 0.3$. Two estimates are illustrated, one using $\mu_0 = 1/(1+\tau l)$ and one with the correction $\mu_0 = 1/(1+(\tau+\tau_b)l)$. We see that the Poisson approximation with the correction term accurately predicts the loss due to blocking with exponential recovery.

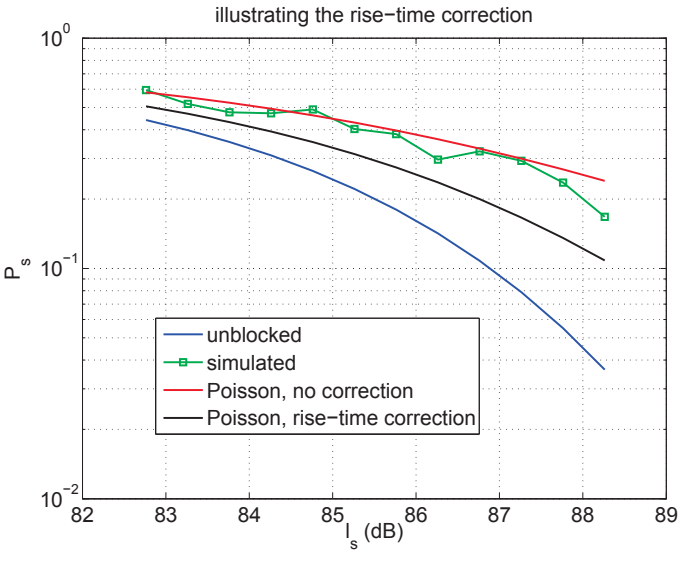

Fig. 8. Estimated Blocking Loss With Exponential Detection Efficiency Recovery

VI. Non-Uniform Intensity Patterns

In the general case, the signal intensity on each detector will be non-uniform. In this section, we consider two non-uniform patterns: a diffraction-limited pattern, and a speckle pattern caused by atmospheric distortion of the signal.

With a non-uniform pattern, one can improve the performance by summing a subset of the detector outputs [9]. In fact, a weighted sum, in the absence of blocking, is a sufficient statistic for the ML receiver. We do not select a subset of the elements here, although the analysis could be extended to include that case. We assume the entire collection of detector outputs are summed, without weighting.

A. Diffraction-limited Intensity Pattern

Let $I(\boldsymbol{\rho})$ be the normalized signal field intensity in the focal plane at radial distance $\boldsymbol{\rho}$. Assume the incident signal is a plane wave. Then the intensity pattern is given by an Airy function

$$I(\mathbf{r}) = \left(\frac{2J_1\left(\frac{\pi D \mathbf{r}}{\lambda F}\right)}{\frac{\pi D \mathbf{r}}{\lambda F}} \right)^2$$

which we will approximate as Gaussian

$$I(x,y) \approx \frac{1}{2\pi\sigma_g^2} \exp\left(\frac{-(x^2+y^2)}{2\sigma_g^2} \right)$$

where $\sigma_g = 1.35\lambda F/(\pi D)$, and $\mathbf{r} = \sqrt{x^2+y^2}$. Let the focal plane be divided into an array of K square pixels, where each pixel has width $2d$, and the jth pixel center is at $(\boldsymbol{\rho}_{j,1}, \rho_{j,2})$. Let the center of the intensity pattern be offset by a radial distance $\mathbf{r}' = (r_1, r_2)$. The fraction of signal power integrated by the jth pixel is

$$q_j = \int_{\rho_{j,1}-r_1-d}^{\rho_{j,1}-r_1+d} \int_{\rho_{j,2}-r_2-d}^{\rho_{j,2}-r_2+d} I(x,y)dxdy$$

Figure 9 illustrates an example with $D = 20$ cm, $F = 1$ m, $K = 25$, $lb = 6.25 \times 10^7$ p/s, $l_d = 10^3$ e/s, $T_s = 128$ ns, $\tau = 2T_s$, $M = 16$, $d = 5 \times 10^6$, and $\eta = 0.5$. Illustrated are the SER for the unblocked case, the blocked simulation, and three estimates of the blocked performance: one using the Poisson approximation with rates given by (5) (6), one using (1)(2) for the slot statistics, and one using (7), with μ_0 set by the detector with the maximum q_j. Since the blocking duration is moderate, the estimate from (1)(2) is accurate. The Poisson approximation is less accurate, since, although K is large, the number of detectors with significant illumination by the signal is small. Finally, (7) accurately tracks the Poisson estimate, simply by choosing the detector with the maximum blockage.

B. Focal Plane Signal Distribution in the Presence of Clear Air Turbulence (Speckled Intensity Patterns)

As a wave propagates through turbulent atmosphere, its phase is distorted. This phase distortion manifests itself at the focal plane of an imaging systems with a point spread function much larger of the of diffraction limit. If the integration time of a pixellated detector or a CCD device at the focal plane is

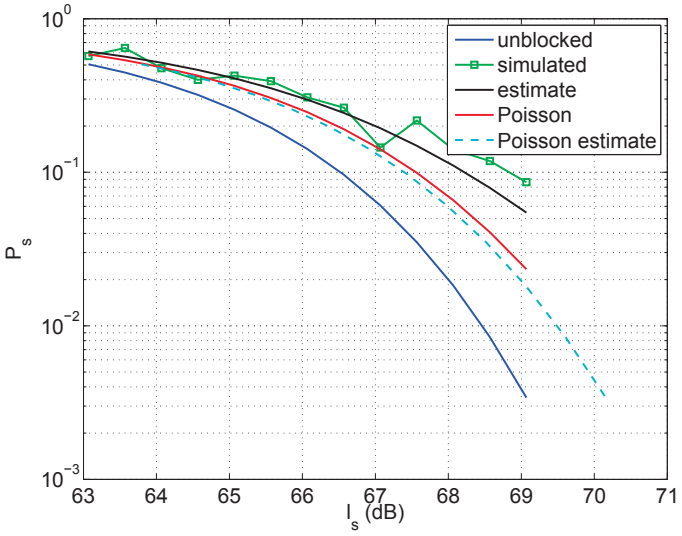

Fig. 9. Symbol Error Rates in Blocking with Airy-pattern Illumination

much less than the atmosphere coherence time, the distribution of light at the focal plane will be essentially speckled. In other terms, the energy content of a downlink signal beam integrated over a slot time will be distributed at the focal plane in a number of speckles, each one of angular extension of a diffraction limited spot [10].

Accurate simulation of the speckled distribution of the signal at the receiver is a problem not easy to describe exactly. One approach is to use Wave-Optics simulation, that simulates the propagation of the signal in a number phase screens, and then image the distorted signal at the focal plane [11]. Wave-Optics simulations, however, are time consuming and problem specific (generalization of results to different problems with dissimilar initial condition are not easy to apply).

However, using a heuristic approach, approximations and some results from clear sky turbulence theory it is possible to have a satisfactory modeling of the problem itself. Considering a downlink signal that is propagating in turbulent atmosphere, the figure of merit that better describes the clear air turbulence and its effects on beam propagation is the atmospheric coherence length, r_0, given by

$$r_0 = \left(0.423k^2 \sec(\theta) \int C_n^2(h)dh\right)^{-3/5} (m)$$

in which k is the wavenumber, for a slant path θ is the angle from zenith, while $C_n^2(h)$ is strength of the turbulence defined as the refractive index structure coefficient along the vertical profile of the atmosphere at altitude h [12] . In first approximation one can describe r_0 as the diameter of a disc where the phase of a propagating wave at wavelength λ (with $k = 2\pi/\lambda$) is approximately constant. The atmospheric coherence length varies during the day (smaller during daytime larger during nighttime) and it is location dependent (larger in mountain top, smaller at sea level). For a good location, the atmospheric coherence length can assume values of tens of centimeters, while for a bad locations it is just few centimeters.

Effects of the clear air turbulence on the imaging system of a telescope are basically described by the ratio given by the telescope diameter D over the atmospheric coherence length [10]. For $D/r_o < 3$ and for short-exposure, the spot size at the focal plane is approximately that of the diffraction limited spread function function. The variation of the angle of arrival (tilt) due to turbulence, will displace the location of the spot at focal plane. For short-exposure we define an integration time (or slot time) is less the atmosphere coherence time τ approximately given by

$$\tau \approx r_0/V$$

where V is the wind speed at ground, with τ usually of the order of milliseconds [13]. For $D/r_o \gg 3$, and for exposure time much larger than τ the full width half maximum of the point spread function at focal plane will angularly given by the astronomical seeing, defined as

$$S_e = \lambda/r_o$$

which is many time the diffraction limits of a telescope [12].

Finally, for $D/r_o \gg 3$ and for integration time less than τ, the short-exposure point spread function is much larger than the diffraction limit (but less than that one given by the astronomical seeing). In this case the point spread function can be described by the a gaussian like function as approximated in [14]. For each realization, the centroid of this point spread function is still displaced over the focal plane by the tilt angle. The signal envelope at the focal plane will be described by a collection of speckles with the number of speckles approximately given by $(D/r_o)^2$, while for each realization the probability of speckle locations at the focal plane will be described by the short-exposure point spread function [10].

Of great interest is the case in which at the focal plane is located a pixellated detector: the overall response of the system will depend on the number of pixels, pixel pitch, and number of speckles. If the number of the speckles is very large in comparison of the number of pixel illuminated, the overall envelope of the pixel response will be similar of that one described by the short-exposure point spread function sampled by detector pixels at the focal plane. If instead, the number of speckles are much less than the number of pixels covered by the short-exposure point spread function, than the overall response envelope will be not continuous, with a limited number of pixels illuminated by one or more than one speckle.

VII. Conclusions

In this paper we have characterized losses on a photon-counting communications link due to detector blocking. We illustrated how to approximate the losses when the output is well characterized as Poisson, as well as numerical methods to evaluate the losses when it is not. The approximate losses allow a simple, accurate, approximation of blocking loss for most cases with a relatively large detector array and sparse event arrival rates.

APPENDIX

In this section, we provide a method to accurately estimate count rates at the detector output for the model of blocking with exponential recovery given by (4). The source is memoryless Bernoulli, producing a pulsed slot, of duration T_s, with probability $1/M$, and a non-pulsed slot with probability $(M-1)/M$. Let n_s and n_b denote the mean un-blocked signal and noise electrons per slot, respectively.

Divide time into sub-slots of duration δ, where, for notational convenience, we assume δ divides τ, τ_b and T_s. The detector behavior may be accurately modeled with the Markov chain illustrated in Figure 10. On this graph, each transition corresponds to a step of duration δ. To simplify notation, throughout this section in evaluating $\eta(t)$ we set the last arrival to be $s = 0$. We approximate $\eta(t)$ as constant over each δ: state i corresponds to a detection efficiency of $\eta(i\delta)$ and state 1 denotes a detection event (and a reset of the detection efficiency). To restrict the number of states to be finite, we do not distinguish differences in the detection efficiency from the maximum when $\eta_0 - \eta(t) < \eta_0\epsilon$, for some $0 < \epsilon < 1$. That is, we put

$$B = \frac{\tau}{\delta}$$
$$U = B - \frac{\tau_b}{\delta}\lceil \ln(\epsilon) \rceil$$

B represents the blocking duration in sub-slots, and U the number of sub-slots required to return to the maximum detection efficiency.

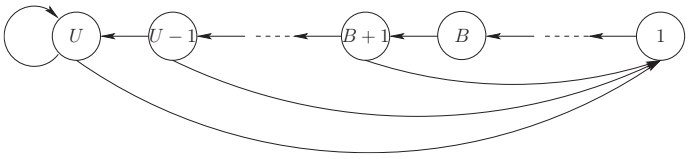

Fig. 10. Discrete-Time Markov Model of Detector

Due to the modulation, transition probabilities are constant for blocks of T_s/δ edges. In order to model this, we define transition matrices Q_0, Q_1 as follows. Let $S(n\delta) \in \{1, 2, \ldots, U\}$ denote the state at time $t = n\delta$ and $X \in \{0, 1\}$ the binary input (the slot is pulsed for $X = 1$ and non-pulsed for $X = 0$). Define the matrices Q_x, $x \in \{0, 1\}$, to have (i, j)-th element

$$[Q_x]_{i,j} = P(S(n\delta) = j | S((n-1)\delta) = i, X = x)$$
$$= \begin{cases} \exp(-(xn_s + n_b)\eta(i\delta)\delta/T_s) & , j = \max(U, i+1) \\ 1 - \exp(-(xn_s + n_b)\eta(i\delta)\delta/T_s) & , j = 1 \\ 0 & , \text{otherwise} \end{cases}$$

Q_1 and Q_0 are the *sub-slot* probability transition matrices for a pulsed and non-pulsed slot, respectively. The *slot* probability transition matrix is given by

$$[Q]_{i,j} = P(S(nT_s = j) | S((n-1)T_s = i)$$
$$= \frac{M-1}{M}[Q_0^{T_s/\delta}]_{i,j} + \frac{1}{M}[Q_1^{T_s/\delta}]_{i,j}$$

The slot probability matrix is aperiodic and irreducible. Hence the state probabilities approach the steady state values $P(S(n) = i) = [\mu]_i$ given by the (normalized) left eigenvector of Q.

$$\mu Q = \mu$$

A. Detected Count Rates

Let k denote the number of counts in a slot, and $k_i, i = 1, 2, \ldots, T_s/\delta$, denote the number of counts in sub-slot i (of duration δ). Assume that $\delta \leq \tau$. Then each sub-slot has at most one count, and the mean count in noise slot may be approximated (up to the discrete-time approximation) as

$$\begin{aligned} \tilde{n}_b &= E[k|x=0] \\ &= \sum_{i=1}^{T_s/\delta} E[k_i|x=0] \\ &\approx \sum_{i=1}^{T_s/\delta} P(S(i\delta = 1)|x=0) \\ &= \left[\mu(Q_o + Q_0^2 + \ldots + Q_0^{T_s/\delta})\right]_1 \end{aligned} \quad (8)$$

(note that $\tilde{n_b}$ is the mean count in blocking, whereas n_b is the mean count if there were no blocking)where $[v]_1$ denotes element 1 of vector $[v]$ (corresponding here to state 1). Similarly, the mean counts in a pulsed slot may be approximated as

$$\begin{aligned} \tilde{n}_s + \tilde{n}_b &= E[k|x=1] \\ &\approx (n_s \hat{+} n_b) = \left[\mu(Q_1 + Q_1^2 + \ldots + Q_1^{T_s/\delta})\right]_1 \end{aligned} \quad (9)$$

Figures 11 and 12 illustrate the count rates in a noise and signal slot from a simulation of the continuous-time model for the parameters corresponding to a single detector in Figure 8: $M = 8$, $T_s = 1$ ns, $l_b = 1.6 \times 10^9$ p/s (a rate of 10^8 per detector), $l_d = 10^3$ e/s, $\eta_0 = 0.3$, $\tau = 8T_s$, $\delta = T_s/4$, $\epsilon = 0.1$, and $\tau_b = 16T_s$. Also illustrated are the estimates (8), (9).

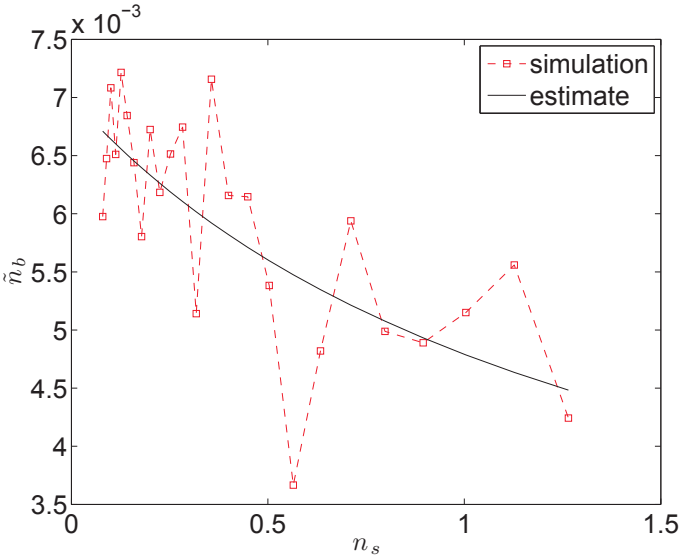

Fig. 11. Count rates in a noise slot: simulated and estimated

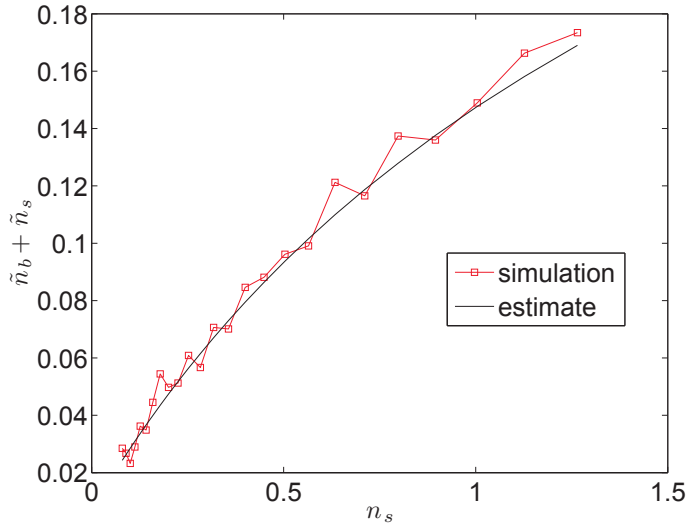

Fig. 12. Count rates in a signal slot: simulated and estimated

ACKNOWLEDGMENT

We would like to thatnk Baris Erkmen for helpful discussions on this material. The research described in this publication was carried out by the Jet Propulsion Laboratory, California Institute of Technology, under a contract with the National Aeronautics and Space Administration.

REFERENCES

[1] C. C. Chen, "Effect of detector dead time on the performance of optical direct-detection communication links," *Telecommunications and Data Acquisition Progress Report*, vol. 42–93, pp. 146–154, January-March 1988.

[2] D. L. Snyder, *Random Point Processes*. Wiley, 1975.

[3] B. Moision and J. Hamkins, "Deep-space optical communications downlink budget: Modulation and Coding," *IPN Progress Report*, vol. 42-154, Aug. 2003.

[4] B. Moision, M. Srinivasan, and J. Hamkins, "The blocking probability of geiger-mode avalanche photo-diodes," in *SPIE* (B. Huang, R. W. Heymann, and C. C. Wang, eds.), vol. 5889, 2005.

[5] I. Kontoyiannis, P. Harremoës, and O. Johnson, "Entropy and the law of small numbers," *IEEE Transactions on Information Theory*, vol. 51, pp. 466–472, feb 2005.

[6] D. M. Boroson, "The communications penalty of refresh times in geiger-mode detectors," tech. rep., MIT-Lincoln Laboratory, April 2004.

[7] A. D. Wyner, "Capacity and error exponent for the direct detection photon channel–Part I," *IEEE Transactions on Information Theory*, vol. 34, pp. 1449–1461, Nov. 1988.

[8] B. Moision, "Capacity of the Poisson PPM channel: Some simple approximations and rules of thumb," tech. rep., Jet Propulsion Laboratory, August 2008. Internal office memorandum.

[9] V. A. Vilnrotter and M. Srinivasan, "Adaptive detector arrays for optical communications receivers," *itc*, vol. 50, pp. 1091–1097, July 2002.

[10] J. W. Goodman, *Speckle Phenomena in Optics: Theory and Applications*. Roberts, 2007.

[11] D. M. Strong, E. P. Magee, and G. B. Lamont, "Implementation and test of wave optics code using parallel FFT algorithms," in *Proceedings of the SPIE*, no. 4167 in 34, 2001.

[12] L. C. Andrews, R. Phillips, and C. Y. Hopen, *Laser Beam Scintillation with Applications*. SPIE Press, 2001.

[13] M. Schoeck and E. J. Spillar, "Analysis of turbulent atmospheric layers with a wavefront sensor: testing the frozen flow hypothesis," in *SPIE* (R. K. Tyson and R. Q. Fugate, eds.), vol. 3762, pp. 225–236, 1999.

[14] L. C. Andrews, R. L. Phillips, R. J. Sasiela, and R. R. Parenti, "Strehl ratio and scintillation theory for uplink Gaussian-beam waves: beam wander effects," *Opt. Eng.*, no. 45, 2006.